Thermochimica Acta, 74 (1984) 291–312
Elsevier Science Publishers B.V., Amsterdam – Printed in The Netherlands

THERMAL AND MÖSSBAUER STUDIES OF IRON-CONTAINING HYDROUS SILICATES. V. BERTHIERINE

K.J.D. MACKENZIE and R.M. BEREZOWSKI
Chemistry Division, DSIR, Private Bag, Petone (New Zealand)

(Received 7 October, 1983)

ABSTRACT

Thermal analysis, X-ray diffraction, infrared and Mössbauer spectroscopy show that Norwegian and Japanese berthierines heated under either oxidising or reducing conditions below ~ 250°C undergo internal oxidation, with an increase in cell dimensions. Re-reduction occurs at ~ 200–400°C under reducing atmospheres. At higher temperatures, dehydroxylation of the specimen containing less aluminium results in the immediate formation of crystalline hematite (in air) or olivine and iron metal (in reducing atmospheres), whereas the more aluminous berthierine behaves like kaolinite, forming an X-ray amorphous phase which persists to 800–900°C before recrystallization. The higher-temperature products in both oxidising and reducing atmospheres include cubic spinel phases and cristobalite, with the more aluminous sample also forming $FeAlO_3$ and mullite in air. No evidence was found for intermediate magnetite formation, as predicted in a previously-suggested reaction sequence.

INTRODUCTION

Berthierine is a hydrous layer silicate with a kaolinite-type 7 Å structure consisting of alternating tetrahedral (Al, Si)–O sheets and trioctahedral brucite-like sheets [1]. In the past, the nomenclature of this mineral has been somewhat confused; the name berthierine was originally given by the French chemist P. Berthier to a variety of chamosite. For some time the latter name took precedence until it became recognised that the type mineral, from the Chamosin district of France, has the 14 Å layer structure of a true chlorite, whereas many minerals of similar chemical constitution from widely differing localities have 7 Å structures. A subsequent suggestion [2] that the 7 Å chamosites be called septechamosites was not wholly satisfactory and the original name berthierine has now become generally accepted for these minerals.

Berthierine can exist in orthohexagonal or monoclinic forms, depending on the stacking sequence of the kaolinite-type layers [1]. The structure is also able to tolerate a predominance of Fe^{3+} or Fe^{2+} ions, giving rise to both ferric and ferrous forms. Ideal ferrous berthierine is structurally related to ideal amesite, $(Mg_4Al_2)(Si_2Al_2)O_{10}(OH)_8$ by replacement of octahedral Mg

0040-6031/84/$03.00

by Fe^{2+}, giving the ideal formula $(Fe_4^{2+}Al_2)(Si_2Al_2)O_{10}(OH)_8$. On gentle thermal oxidation, the octahedral ferrous ions can be almost completely converted to ferric, without loss of the berthierine structure, but with conversion of OH^- to O^{2-} to maintain charge balance [3].

A previous X-ray study of the thermal reactions of a British berthierine [3] suggests that in air, simultaneous dehydroxylation and oxidation result in the formation of an amorphous phase at ~ 450–500°C. Recrystallization of hematite commences at ~ 550°C, with spinel, $MgAl_2O_4$ and cristobalite, SiO_2, appearing at 800 and 900°C, respectively. In steam atmospheres and under reduced pressure, oxidation is suppressed; recrystallization to $FeAl_2O_4$ is said to occur in steam at 650°C without the formation of an amorphous intermediate, whereas in vacuum, an amorphous phase formed at 350°C recrystallized to poorly crystalline $FeAl_2O_4$ [3].

A more recent thermomagnetic study of a different berthierine in air and vacuum [4] suggested a mechanism in which Fe^{2+} migrates during dehydroxylation along the dislocations appearing throughout the structure, followed by oxidation to magnetite concomitant with hydroxyl loss

$$3\ Fe^{2+} + 6\ OH^- \rightarrow Fe_3O_4 + 2\ H_2O + H_2 \qquad (1)$$

In air, the magnetite was thought to be subsequently oxidised to hematite, Fe_2O_3, the remainder of the ferric iron forming the spinel $MgFe_2O_4$, identified by its Curie point [4].

Mössbauer spectra of five berthierines have been reported. Weaver et al. [5] published the spectrum of an undescribed specimen consisting of an octahedral Fe^{2+} doublet with a smaller Fe^{3+} peak ascribed to iron oxide impurities; an essentially similar spectrum has more recently been published for a French berthierine [6]. A Mössbauer study of three Russian berthierines [7] has shown two pairs of ferrous doublets corresponding to non-equivalent octahedral sites and a small ferric doublet. In the Russian samples heated in air to 400°C, the Fe^{2+} in the more distorted sites were the most readily oxidised [7]. The thermal transformations at higher temperatures and in other atmospheres have not been studied by Mössbauer spectroscopy. No IR studies of heated berthierines have been reported.

The aim of the present work was to investigate the thermal transformations of well-characterized berthierines in both oxidising and reducing conditions, using a number of experimental techniques which have provided useful information in studies of related minerals [8].

EXPERIMENTAL

Materials

One of the two berthierines studied here was from specimen BM34121 of the British Museum collection, and came from the Kongeus Mine, Kongs-

berg, Norway. A previous X-ray study [1] has shown that this material, designated B1 in the present paper, is predominantly of the orthohexagonal form, with only about 10% of the monoclinic form present. The chemical analysis (by atomic absorption spectroscopy) and the calculated structural formula are shown in Table 1. Semi-quantitative arc-spectral analysis showed this sample to be particularly free of trace impurities.

The second berthierine, designated B2, was from a berthierine–quartz rock, specimen 76-12-1B, from Hiramatsu, Utatsu, Miyagi, Japan, and is described in detail elsewhere [9]. X-ray powder diffraction indicates that this material contains only well-crystallized berthierine and quartz. The electron microprobe analysis of the berthierine phase is given in Table 1. Comparison of the electron microprobe results with the chemical analysis of the whole rock [9] indicates a quartz content of ~ 12%, but X-ray powder diffraction suggests a higher quartz content in the present material. TG analysis (next section) is consistent with ~ 28–37% of non-berthierine component. Attempts to separate the berthierine from the quartz were unsuccessful due to the fine-grained intergrowth of the two phases, and the present work was therefore carried out on the whole material.

Methods

The samples were reacted both in still air and dynamic atmospheres of 5% H_2/95% N_2 by a serial heating method previously described [8]. After holding the samples at various temperatures, chosen with reference to the DTA curve obtained under the appropriate atmosphere, the progress of the reaction was monitored by X-ray powder diffraction, IR spectroscopy and Mössbauer spectroscopy using an Elscint AME 40 Mössbauer spectrometer. Other experimental details are described elsewhere [8].

RESULTS AND DISCUSSION

(a) Thermal analysis

DTA traces of the two berthierines under oxidising, inert and reducing atmospheres are shown in Fig. 1. The traces of both samples in air (Fig. 1, curves A and G) differ from those in inert and reducing atmospheres, the latter containing one or more dehydroxylation endotherms followed by exothermic features of various intensities (curves B, C, H and I). The DTA traces of both samples in air are dominated by a large, broad exotherm at ~ 300–400°C (curves A and G) due to the oxidation of ferrous iron, a reaction which obscures the dehydroxylation endotherms, particularly in B1. This result is at variance with the two previously-reported DTA traces of berthierines [1,10], in which the atmosphere, although unspecified, was

TABLE 1

Chemical analyses and unit cell contents of berthierines

Component	1 [a]		2 [b]		Unit cell contents		1 [a]		2 [b]		3 [c]	
SiO_2	25.46		22.87		Si	Td	2.98	4.0	2.60	4.0	2.0	4.0
Al_2O_3	10.99		23.24		Al	Td	1.02		1.40		2.0	
Fe_2O_3	26.25		40.15		Al	Oh	0.48	5.28	1.72	5.83	2.0	6.0
FeO	20.20				Fe^{3+}	Oh	2.30					
CaO	0.93		0.09		Fe^{2+}	Oh	1.96		3.81		4.0	
MgO	2.45		1.77		Ca	Oh	0.14		0.01			
K_2O	0.21		0.00		Mg	Oh	0.40		0.29			
Na_2O	0.20		0.00		OH		7.66		8		8	
TiO_2	0.09				O		10		10		10	
MnO	0.13											
$H_2O(-)$	3.60	13.40	11.88 [d]									
$H_2O(+)$	9.80											
Total	100.13		100.00									

[a] Column 1. Berthierine B1, specimen BM 34121, Norway. Analyst: M.W. Dwyer.
[b] Column 2. Berthierine B2, specimen 76-12-1B, Japan. Analyst: H. Haramura [9].
[c] Column 3. Ideal ferrous berthierine.
[d] Water content by difference.

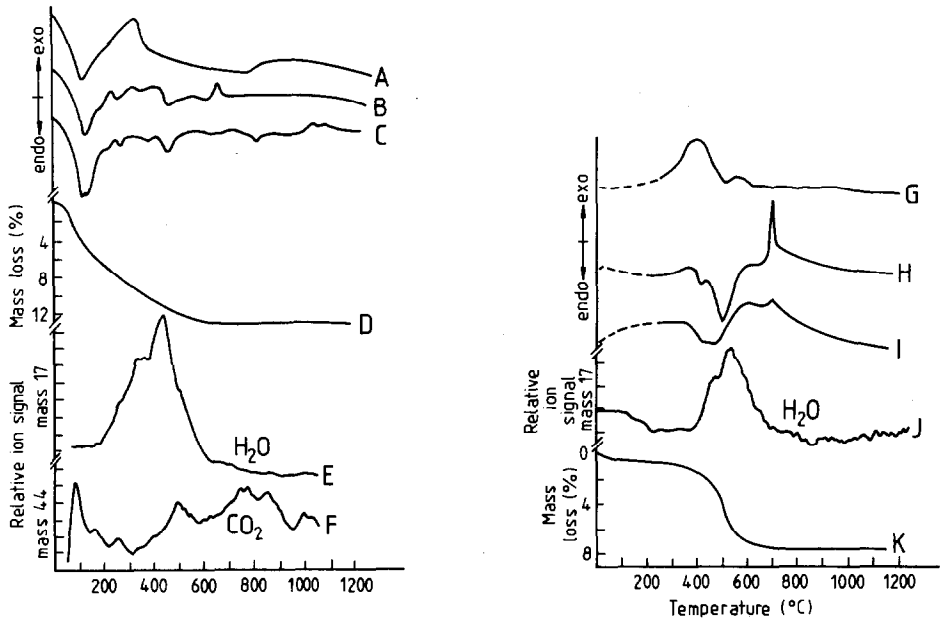

Fig. 1. Thermal analysis of berthierines. Heating rate 10°C min^{-1}. Curves A–F, berthierine B1 (Norway). A, DTA in air; B, DTA in H_2/N_2; C, DTA in oxygen-free N_2; D, TG in oxygen-free N_2; E, EGA, mass 17 (water); F, EGA, mass 44 (CO_2). Curves G–K, berthierine B2 (Japan). G, DTA in air; H, DTA in H_2/N_2; I, DTA in oxygen-free N_2; J, EGA, mass 17 (water), no other gaseous species detected; K, TG in air. Dashed portions of curves G, H and I indicate region where background was subtracted to counteract the effect of baseline drift.

probably air. The main feature of both the earlier DTA results was a dehydroxylation endotherm at ~ 550°C; in the French berthierine [10] this was followed by a sharp exotherm at ~ 650°C, with some higher-temperature peaks being ascribed to (unspecified) impurities. The absence of an oxidation exotherm in the earlier work could be understood if the sample holder retained the self-generated atmosphere instead of permitting a dynamic gas flow around the sample, as in the present experiments.

Low-temperature endotherms were observed in sample B1 in all atmospheres (curves A, B and C) and correspond to a rapid weight loss (curve D). However, the major weight-loss in B1 is more gradual, extending over ~ 400°C and apparently incorporating up to three endothermic events (curves B and C). The explanation for this behaviour is apparent from the EGA curves, obtained using an Extranuclear quadrupole mass spectrometer with helium carrier gas, the results of which indicate that in addition to the loss of hydroxyl water at 300–400°C (Fig. 1, curve E), small amounts of CO_2 are also evolved at about 100, 500 and 750–850°C (curve F), probably resulting from the decomposition of carbonate impurities, the concentrations of which are too small to be detected by X-ray diffraction. The CO_2 evolution at ~ 100°C appears more likely to be due to the release of gas entrained in the porous structure or adsorbed on the surface of the particles.

No other evolved gas species was detected. The nett result is a rapid initial endothermic CO_2 weight loss followed by a more gradual weight loss due to dehydroxylation and decarboxylation, the former accounting for the endotherm at ~ 500°C, while the other smaller endotherms in B1 probably reflect decarboxylation events.

The initial portions of the DTA traces of B2, shown as broken lines in Fig. 1, curves G, H and I, were subject to baseline drift in the micro DTA sample holder; the baselines in this region were independently established and subtracted from the traces. No low-temperature thermal events analogous to those in B1 were found for B2. The TG curve for B2 (curve K) indicates a much sharper water-loss step than for B1, as is also reflected in the more intense endotherms under all atmospheres. The EGA results for B2 (curve J) indicate that water is the only species evolved, being lost in two stages corresponding to the double endotherm which is particularly well resolved under reducing conditions (curve H). A similar two-stage water loss is also discernible in B1 (curve E). It appears likely that one of the two water-loss mechanisms thus indicated involves internal oxidation

$$Fe^{2+} + OH^- \rightarrow Fe^{3+} + O^{2-} + H^{\cdot} \quad (2)$$

where the hydrogen atoms thus produced react with any available oxygen to form water [3]. The second mechanism occurs either when all the available Fe^{2+} has been oxidised, or when the temperature is sufficiently elevated

$$2\,OH^- \rightarrow O^{2-} + H_2O \quad (3)$$

The relative contributions of these mechanisms in the present reactions cannot be estimated by thermal analysis because (a) the overlapping EGA peaks preclude the necessary quantification, and (b) the redox behaviour of these berthierines is complex, being shown by Mössbauer spectroscopy [see section (d)] to involve the creation or destruction of more than one ferrous site.

The total weight loss found for B2 was 7.5%, whereas the microprobe analysis for the berthierine component (Table 1) indicates an expected water content of 11.9% (by difference), in reasonable agreement with the theoretical water content of ideal berthierine (10.5%). Thus, 63.1% of B2 must be composed of berthierine, the balance being quartz. The berthierine content of B2, as estimated by TG, is less than the estimate given by Iijima and Matsumoto [9] for this sample (77–84%), and indicates a rather variable quartz content in this berthierine rock.

(b) X-ray diffraction

The X-ray traces of the unheated berthierines show B1 to be considerably less crystalline than B2, which is, however, significantly contaminated with quartz and also contains a very small peak at 14.5 Å due to a chloritic phase

which is not detected in B1. Sample B2 shows a diffuse reflection at 2.423 Å, probably due to the presence of a small amount of poorly crystalline monoclinic berthierine, for which a line at 2.404 Å is said to be diagnostic [3]. Sample B1 is predominantly in the orthohexagonal form [1].

On heating under both oxidising and reducing conditions, the d-spacings of both berthierines decrease, reflecting contractions in the cell dimensions due to oxidation. Under oxidising conditions, conversion to the ferric form, as indicated by cell contraction, is complete by ~ 400°C; under reducing conditions, the partially oxidised form begins to be reduced at 200–300°C, reverting to the fully ferrous cell dimension by 350–400°C. The d-spacings of these samples, measured using the quartz peak as an internal angular calibrant, were indexed on the basis of the orthohexagonal cell of Brindley and Youell [3] ($a = 5.415$ Å, $b = 9.379$ Å, $c = 7.114$ Å), allowing the cell parameters to be refined using the computer program of Evans et al. [11]. On oxidation to the fully ferric form, B1 undergoes a 2.5–2.8% contraction in the a and c parameters, but the b parameter contracts by only 0.4%, by contrast with the findings of Brindley and Youell [3] of ~ 3% contraction in the a and b dimensions, the c parameter contracting by 0.75%. A still different result was found for B2, in which the a and b parameters contract by 0.3–0.5% and the c parameter by 2% on oxidation. Variability in the cell parameters of oxidised berthierine is further demonstrated by the findings of Kodama and Foscolos [12] that samples from arctic desert soils undergo a 2.2% contraction in the b parameter on heating to 300°C. Although the b parameters of unheated B1 and B2 (9.383 Å and 9.360 Å, respectively) are similar to those previously reported for the ferrous form (9.38 Å [3]), their values after oxidation (~ 9.33 Å) are larger than found by Brindley and Youell [3] or Kodama and Foscolos [12] (~ 9.10 Å). Two possible explanations are (i) the present heating conditions were such that oxidation did not proceed to completion before being overtaken by structural breakdown due to dehydroxylation, or (ii) the presence of substantial numbers of octahedral cations other than Fe^{2+} might interfere with the collapse of the b parameter. Despite differences in detail, however, all the parameters of B1 and B2 behave consistently on progressive oxidation or reduction, as seen in the change of calculated cell volumes with reaction temperature (Fig. 2).

Figure 2 shows a 5.6% contraction in the cell volume of B1 on oxidation, in reasonable agreement with the 6.6% contraction reported by Brindley and Youell [3] for a different sample. The smaller contraction of B2 (2.6%) is largely due to a much smaller contraction in its a parameter. The initial internal oxidation indicated by the cell volume changes under reducing conditions were confirmed by Mössbauer spectroscopy [section (d)]; similar behaviour was also noted in cronstedtite [13].

At ~ 200°C in both oxidising and reducing atmospheres, the weak 14 Å chloritic reflection in B2 becomes more intense; under oxidising conditions, this reflection persists for at least another 200°C after the 7 Å berthierine

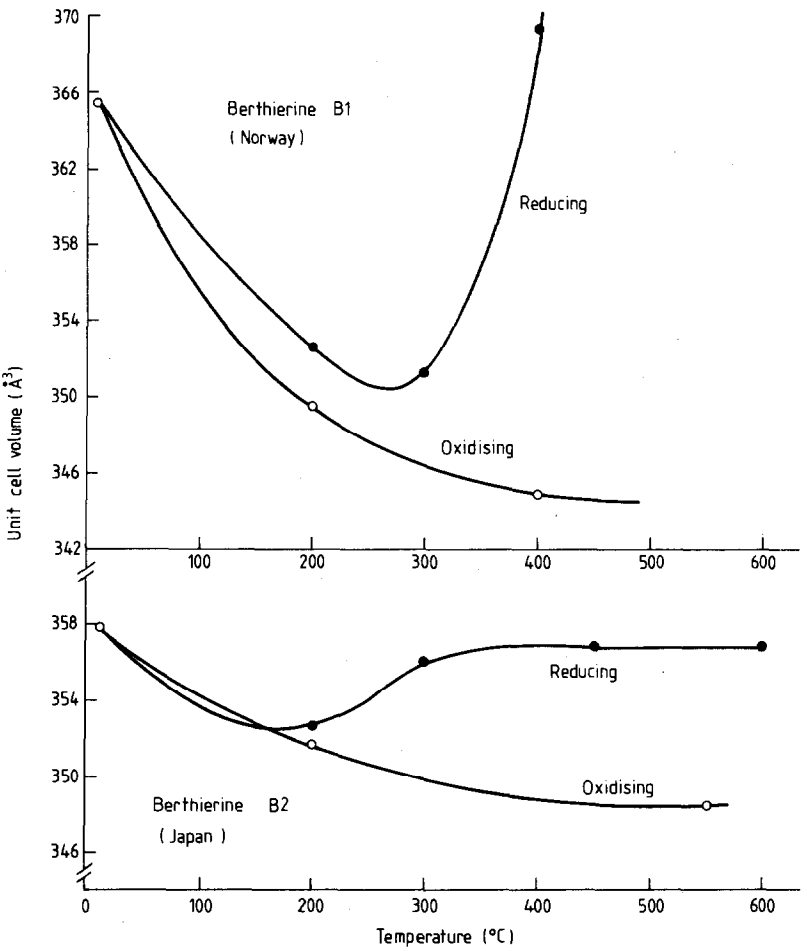

Fig. 2. Changes in X-ray cell volume of berthierines as a function of heating temperature.

reflection has been destroyed (at ~ 600°C). Under reducing conditions, the 14 Å reflection disappears simultaneously with the 7 Å phase. No 14 Å phase developed in B1 on heating. The appearance of a 14 Å phase during heating has been reported in amesite [8,14] and in other 7 Å chlorites [14], but not in 7 Å chamosite (berthierine), which became X-ray amorphous in the previous study after heating to the arbitrary test temperature (590°C) for 0.5 h [14]. This finding for berthierine was in part ascribed to its fine particle size [14] and a similar explanation may apply to the present appearance of a 14 Å phase in B2 but not in B1. Alternatively, the 14 Å phase in B2 may simply be an adventitious impurity.

On heating B1 to > 400°C in air, hematite progressively forms at the expense of ferric berthierine. No X-ray evidence of the intermediate formation of magnetite was found, as required by the mechanism of Escoubes and Karchoud [4]. Under reducing conditions, recrystallization is more abrupt,

the products being an olivine and iron metal. At higher temperatures in air, cristobalite and a cubic Fe–Mg–Al spinel appear. By contrast, the cubic phase which occurs under reducing conditions is a transitory ferrous magnesium silicate, $(Mg, Fe)_2SiO_4$, which is replaced by ferrous cordierite, $(Mg, Fe)_2Al_4Si_5O_{18}$, above ~ 1100°C. These changes are shown schematically in Fig. 3.

The behaviour of B2 on heating differs from that of B1 in several ways: (i) A 14 Å phase increases in intensity, as discussed above; (ii) over the

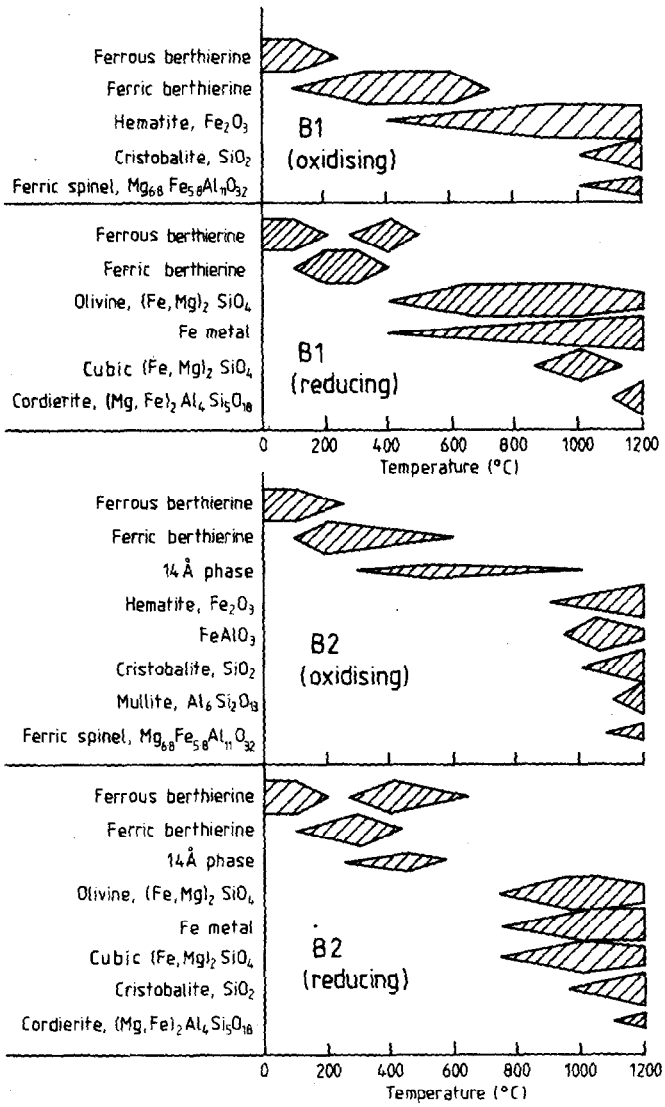

Fig. 3. Schematic representation of phase formation in berthierines as a function of temperature under oxidising and reducing conditions.

temperature range 600–800°C the material is X-ray amorphous; and (iii) consistent with the higher aluminium content of B2, the products in air are more aluminian, and include $FeAlO_3$ and mullite ($Al_6Si_2O_{13}$). As with B1, the high-temperature products of B2 include the cubic phases $(Mg, Fe)_2SiO_4$, under reducing conditions, and an iron(III)-substituted spinel in air. Although precise identification of such spinels is difficult due to similarities in their X-ray patterns, the cell constant of this spinel suggests that it closely resembles $Mg_{6.8}Fe_{5.8}Al_{11}O_{32}$ (JCPDS card No. 21-540).

(c) Infrared spectroscopy

Typical IR spectra of unheated and heated B1 and B2 are shown in Fig. 4. The spectra of unheated B1 and B2 (Fig. 4A and B) are similar to each other, if account is taken of the quartz in B2, and also closely resemble published spectra of arctic desert berthierine [12] and an "impure chamosite" [15]. The spectrum of B1 is broader and less well resolved than that of B2, consistent with the poorer crystallinity of the former. In the hydroxyl stretching region (3400–3600 cm^{-1}) only two broad peaks are resolved in B1, at 3410 and 3545 cm^{-1}, which, by analogy with related amesites are probably due to outer hydroxyl vibrations [16]. The two vibrations pertain to hydroxyl groups bonded to Al–O and Si–O and have previously been cited as evidence for random substitution of Si by Al [16]. Sample B2 also shows a well-resolved band at 3615 cm^{-1}, arising from the vibration of inner hydroxyl groups [14], and which is not resolved in the spectrum of B1.

The following assignments of the other spectral bands are made by analogy with related iron-containing layer silicates [13,17]: 990–1005 cm^{-1}, Si–O stretch; 660–670 cm^{-1}, another Si–O vibration which is shifted to lower frequencies by increasing Fe^{3+} concentration; 530–630 cm^{-1}, M^{3+}–O–Si vibrations, the higher frequency bands corresponding to Al^{3+} and the lower frequency to Fe^{3+}; 450–460 cm^{-1}, Si–O bend; 425 cm^{-1}, Fe^{2+}–O–Si (this band is better resolved in B2 which contains more Fe^{2+}); bands below 400 cm^{-1}, combinations of Si–O, M–O–Si and hydroxyl bending modes. Neither berthierine show much evidence of the band at ~ 930 cm^{-1}, diagnostic of ordered tetrahedral Al-for-Si substitution [16]. The shoulder at 750 cm^{-1} in B2 is characteristic of 14 Å chlorites (ref. 18, chap. 15), and suggests the presence of a small amount of this phase even before thermal treatment improves its crystallinity sufficiently for it to be distinguished by X-ray diffraction. The small, poorly-resolved band at 810 cm^{-1} in B1 is probably an $Fe^{3+} \cdots OH$ vibration; in amesite, this band was assigned to tetrahedral AlO_4 [16], whereas in arctic berthierine it was attributed to a glauconite impurity [12]. A more recent assignment of this band and the shoulder at 720–750 cm^{-1} arises from a deuteration study [19] and suggests that these features are due to (SiAl)O–OH and (SiSi)O–OH vibrations, respectively. This work [19] also associates at least one of the

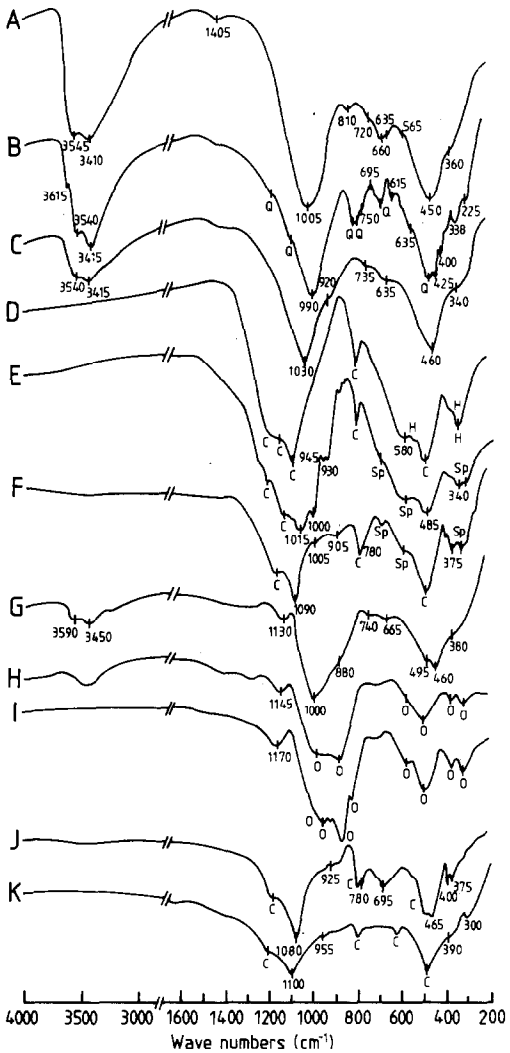

Fig. 4. Typical IR spectra of unheated and heated berthierines. A, Sample B1 (Norway), unheated; B, sample B2 (Japan), unheated; curves C–F, heated in air, curves G–K, heated in H_2/N_2. C, B1, 200–700°C; D, B1, 1050°C; E, B1, 1200°C; F, B2, 1200°C; G, B1, 400°C; H, B1, 550°C; I, B1, 700°C; J, B1, 1200°C; K, B2, 1200°C. Key: Q = quartz; C = cristobalite; H = hematite; Sp = spinel; O = olivine.

bands at 630–660 cm^{-1} with a hydroxyl group; characteristically ferrous chlorites contain two such bands [19] (Fig. 4A and B). The 810 cm^{-1} band in B2 is masked by the strong quartz bands at 780 and 800 cm^{-1}. The presence of carbonate impurity in B1 is confirmed by the ν_3 carbonate vibration at ~ 1400 cm^{-1}; other carbonate bands may contribute to the broad feature at 810 cm^{-1} and the shoulder at 720 cm^{-1} in B1 (Fig. 4A).

On heating in air, the spectra of both berthierines become progressively

broader and more diffuse (Fig. 4C). The well-resolved Fe^{2+}–O–Si band at 425 cm^{-1} is lost from B2, the band at ~ 660 cm^{-1} is displaced to ~ 635 cm^{-1}, and a shoulder at 920 cm^{-1} intensifies, all these features being consistent with increased occupation of tetrahedral sites by Fe^{3+} [17]. Thus, Fig. 4C corresponds to the spectrum of fully oxidised berthierine. A similar spectrum, minus the hydroxyl vibrations, is found for dehydroxylated berthierine. By about 1000°C, the major bands of the recrystallization products (cristobalite and hematite) appear (Fig. 4D), but no indication is found of the diagnostic magnetite band at 390 cm^{-1} at any stage of the reaction in air, militating against the mechanism of Escoubes and Karchoud [4]. Heating in air at 1200°C produces additional new bands in both berthierines. One group, at about 780, 695, 590 and 300 cm^{-1} resembles spinel ($MgAl_2O_4$), and is well developed in B2, which was found by X-ray diffraction to contain appreciable chlorospinel (Fig. 4F). Of more interest are new peaks in the Si–O stretching region which are particularly strong in B1 (Fig. 4E). The bands at 1000 and 900–940 cm^{-1} suggest an olivine (Mg_2SiO_4) or garnet ($Mg_3(Al,Fe)_2(SiO_4)_3$); these phases have similar spectra (ref. 18, chap. 13), the lower-frequency bands of which could also be present in B1 and B2. The lack of X-ray evidence for either of these phases indicates that their concentration is low (< 3%).

Under reducing conditions, B1 at 200°C shows a typical oxidised spectrum (Fig. 4C), but above ~ 300°C the major Si–O peak at ~ 1000 cm^{-1} shifts downwards towards its unheated (ferrous) position. A shoulder which develops at 890 cm^{-1} (Fig. 4G) also indicates increasing substitution of tetrahedral Fe^{2+} for Fe^{3+} [17]. By 550°C, this 890 cm^{-1} peak has become part of a well-developed olivine spectrum (Fig. 1H). Another broad peak at 1120 cm^{-1} develops in B1 and persists to ~ 1000°C; its origin is not certain, but it may be similar to a dioctahedral Si–O vibration noted by Farmer as being sensitive to structural disorder (ref. 18, p. 350). This assignment is consistent with the disorder resulting from trioctahedral ferrous berthierine becoming dioctahedral on oxidation [12], but it does not explain the absence of this band in purposely fully oxidised samples. By 1000°C, the spectrum contains well-developed olivine and cristobalite bands, although the concentration or crystallinity of the latter never becomes sufficient for its detection by X-ray diffraction. Another band at 695 cm^{-1} (Fig. 4J) may indicate the presence of a phase similar to the β-form of olivine. This phase contains oxygens in approximately cubic close-packed array, with cations in octahedral and tetrahedral interstices, as in the spinel structure, but by contrast to the SiO_4 units in silicate spinels, the β-phase contains Si_2O_7 units, for which the diagnostic symmetric stretching frequency occurs at ~ 686 cm^{-1} [20]. Although both the silicate spinel $(Mg, Fe)_2SiO_4$ proposed as a transitory phase in section (b) and its β-form are known only from high-pressure synthetic studies, the occurrence of related cubic close-packed silicon-containing structures may be possible in reaction sequences of layer

silicates, which have a strong tendency to form cubic intermediates.

Heating B2 to < 450°C in H_2/N_2 produces little change in the spectra. At dehydroxylation, several hydroxyl-related vibrations disappear and the spectra broaden, with the appearance of olivine-like bands at 1000°C. At 1200°C, the spectrum of B2 (Fig. 4K) is similar to that of B1, but is less well resolved and does not contain the β-olivine band at 695 cm^{-1}. To summarise the IR results:

(i) Heating B1 and B2 in air below the dehydroxylation temperature produces spectral frequency shifts characteristic of ferric-for-ferrous substitution.

(ii) The major spectral features survive dehydroxylation and persist to ~ 1000°C, when new bands characteristic of some of the product phases appear.

(iii) No spectral evidence is found for the formation of magnetite as an intermediate in the thermal reactions in air.

(iv) In H_2/N_2, the B1 spectra indicate initial oxidation followed by reduction, but no such effect is seen in B2.

(v) Under H_2/N_2, the development of a broad feature at ~ 1130–1170 cm^{-1} in B1 but not in B2 may result from lattice disorder in the former.

(vi) A 695 cm^{-1} band which develops under H_2/N_2 at > 1000°C in B1 but not in B2 may indicate the presence of some olivine in the β-form.

(d) Mössbauer spectroscopy

The room-temperature Mössbauer spectra of unheated B1 and B2 are shown in Fig. 5. Sample B1 contains considerably more ferric iron than B2, located in two ferric sites. Attempts to fit more than one ferrous doublet did not significantly improve the fit to either B1 or B2. The Mössbauer parameters of the unheated samples are shown in Table 2, together with published parameters for other berthierines, related septechlorites and true chlorites.

Table 2 shows that the Mössbauer parameters of all these minerals are remarkably similar, particularly for the ferrous site of major occupancy, which in the 14 Å chlorites has been identified as an octahedral site associated with *cis*-hydroxyl groups in the 2:1 layer [21–23]. Two ferrous doublets were fitted to the Russian berthierines [7], the site of major occupancy and largest QS being assigned to the M1 octahedral site, with minor occupancy of the M2 octahedral site. The ferric sites in berthierines and related minerals fall into two categories: (i) those with IS = 0.21–0.39 and QS = 0.53–0.78 mm s^{-1}, which in the 14 Å chlorites have been assigned to tetrahedral sites [23]; and (ii) those with IS = 0.33–0.53 and QS = 0.82–1.40 mm s^{-1}, which are probably octahedral sites having various degrees of distortion.

The room-temperature Mössbauer spectra of B1 and B2 heated to various temperatures in air are shown in Fig. 6.

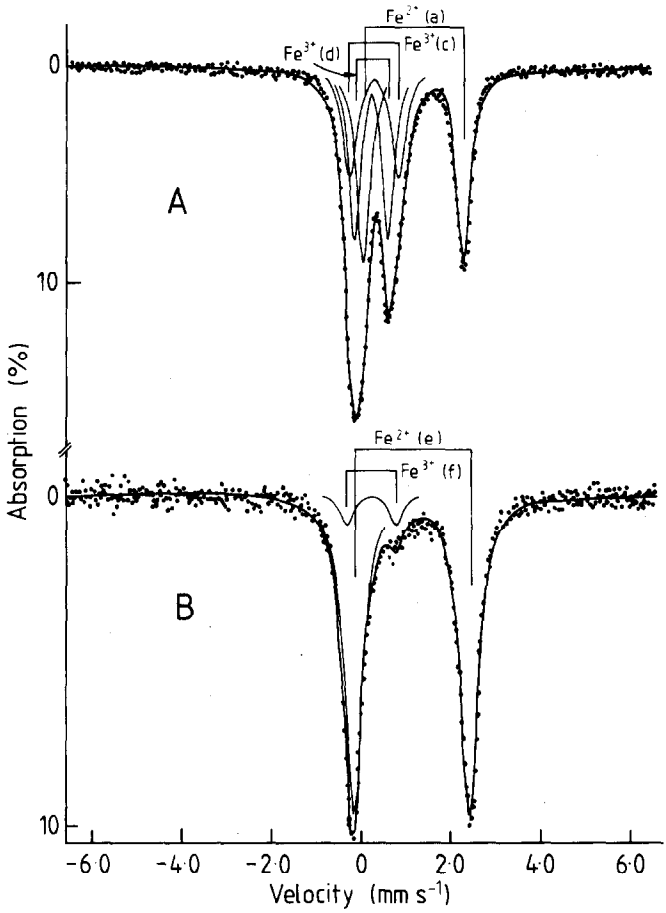

Fig. 5. Room-temperature Mössbauer spectra of unheated berthierines. Source: Co/Rh. A, Sample B1 (Norway); B, sample B2 (Japan).

Figure 6 shows that the appearance and disappearance of the various doublets follows a complex pattern; to clarify the details of the changes in occupancy of the various sites, these have been plotted in Fig. 7 as a function of the heating temperature, on the assumption that the recoil-free fraction of iron in each site is approximately equal, allowing the site occupancies to be estimated from the areas under the computer-fitted peaks. In Fig. 7 and in the following discussion, the various doublets are labelled a, b, etc.

Heating B1 in air at 200°C completely oxidises the octahedral Fe^{2+} resonance a, producing an Fe^{3+} doublet with QS = 1.50–1.75 mm s^{-1}, typical of a highly distorted octahedral site. The Fe^{3+} sites c and d which were initially present, retain their intensities up to about 700°C, when a 6-line hematite spectrum appears at the expense of the Fe^{3+} c sites. Hematite then continues to grow at the expense of the oxidised (originally Fe^{2+}) resonance b, which eventually disappears by ~ 1000°C. The original Fe^{3+}

TABLE 2

Room-temperature Mössbauer parameters of berthierines and related septechlorites and chlorites. Isomer shifts relative to soft iron

Sample	Fe^{2+}		Fe^{3+}		Ref.
	IS	QS	IS	QS	
Berthierine B1 (Norway)	1.22	2.25	0.33	1.11	This work.
			0.26	0.76	
Berthierine B2 (Japan)	1.13	2.58	0.25	1.09	This work.
Berthierine (France)	1.13	2.57	0.38	0.78	6
Berthierine (U.S.S.R.)	1.13	2.78	0.21	0.97	7
	1.16	2.43			
Amesite (2 samples)	1.11–1.13	2.59–2.61	0.35	0.57	8
Cronstedtite	1.21	2.23	0.69	0.79	13
			0.23	0.52	
14 Å chlorite (ripidolite)	1.13	2.60	0.46	0.84	21
			0.39	0.58	
14 Å chlorite (3 samples)	1.13–1.14	2.62–2.64	0.38–0.39	0.56–0.61	22
14 Å chlorite (9 samples)	1.13–1.14	2.68–2.72	0.34–0.47	0.82–1.40	23
	1.12–1.15	2.30–2.51	0.24–0.39	0.53–0.78	
14 Å chlorite, U.S.S.R. (2 samples)	1.25–1.26	2.68	0.50–0.53	0.56–0.80	24

site d, which in 14 Å chlorites has been identified with tetrahedral Fe^{3+} [23], survives at reduced intensity up to 1200°C.

The air oxidation of B2 proceeds less readily than for B1, the original Fe^{2+} doublet e being replaced by two new Fe^{3+} doublets g and h (Fig. 7). At about the dehydroxylation temperature, the two new sites g and h can no longer be distinguished; Fig. 7 suggests that this is due to their coalescence rather than to the abrupt disappearance of site g, a possibility which cannot, however, be completely ruled out. The appearance of hematite at > 700°C is at the expense of the Fe^{3+} resonances f and h, both of which, however, persist up to 1200°C (Fig. 7).

Thus, the behaviour of the iron is similar in both berthierines heated in air, and involves the early oxidation of Fe^{2+} to Fe^{3+}, which in B1 is located in a highly distorted octahedral site. In B2, in which appreciable Fe^{3+} is not originally present, two new Fe^{3+} sites (g and h) can be resolved, the parameters of g corresponding with those of site b in B1. Neither berthierine shows any abrupt change in the Mössbauer spectrum due to dehydroxylation, rather, a gradual decline in the intensity of the Fe^{3+} resonances sets in after dehydroxylation is complete. Hematite grows in both berthierines at

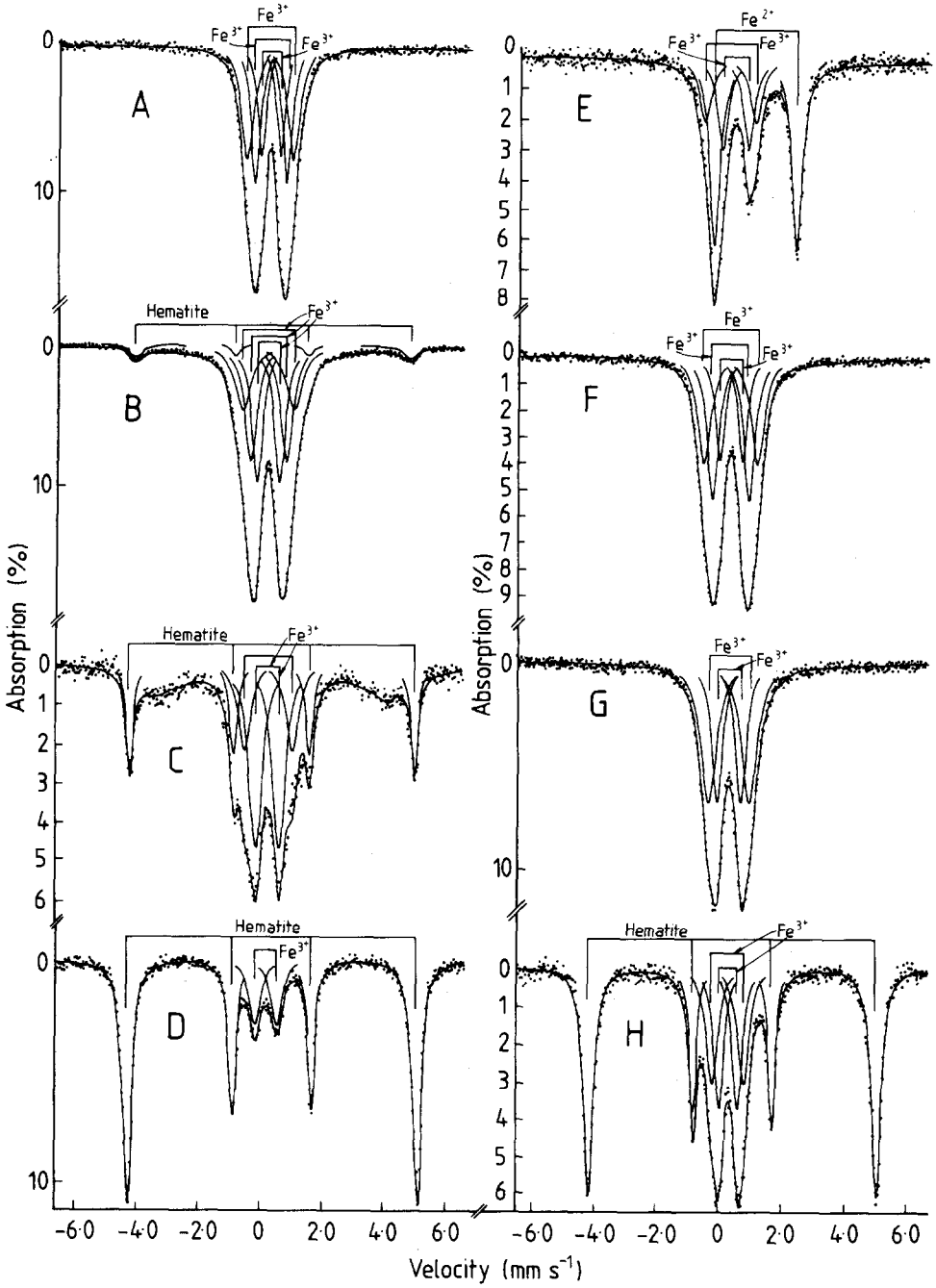

Fig. 6. Typical room-temperature Mössbauer spectra of berthierines heated in air. A–D, Sample B1 (Norway); E–H, sample B2 (Japan). A, 200–400°C; B, 700°C; C, 850°C; D, 1050–1200°C; E, 200–400°C; F, 450–550°C; G, 700°C; H, 1050–1200°C. Outer peaks of hematite spectrum not observed in this velocity range.

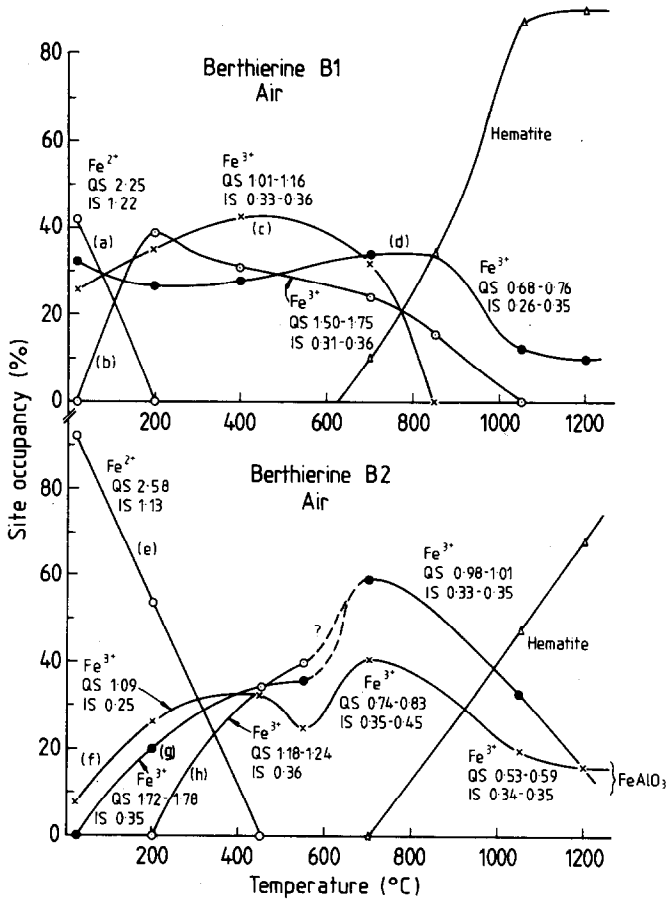

Fig. 7. Iron site occupancy changes in berthierines heated in air, deduced from Mössbauer peak areas. Isomer shifts quoted with respect to iron metal.

the expense of all Fe^{3+} sites, which, however, persist up to 1200°C. The Fe^{3+} doublet persisting in B1 appears to have evolved from the original Fe^{3+} doublet d, which, by analogy with the 14 Å chlorites, may be a tetrahedral site [23]. The X-ray results suggest that this doublet is associated with a cubic Mg–Al–Fe spinel, for which no Mössbauer data have been reported, but which could feasibly contain tetrahedral Fe^{3+}. The Fe^{3+} doublets in B2 heated to 1200°C have identical parameters to those found for pure $FeAlO_3$ (IS = 0.34, QS = 1.06 and 0.53 mm s^{-1}) [25], thus confirming the X-ray identification of this phase in B2.

The room-temperature Mössbauer spectra of B1 and B2 heated to various temperatures under reducing conditions are shown in Fig. 8, the corresponding changes in site occupancy being shown in Fig. 9.

Both berthierines undergo initial oxidation of the original Fe^{2+} site, confirming the X-ray results [section (b)]. In B1, a transient Fe^{3+} species in a

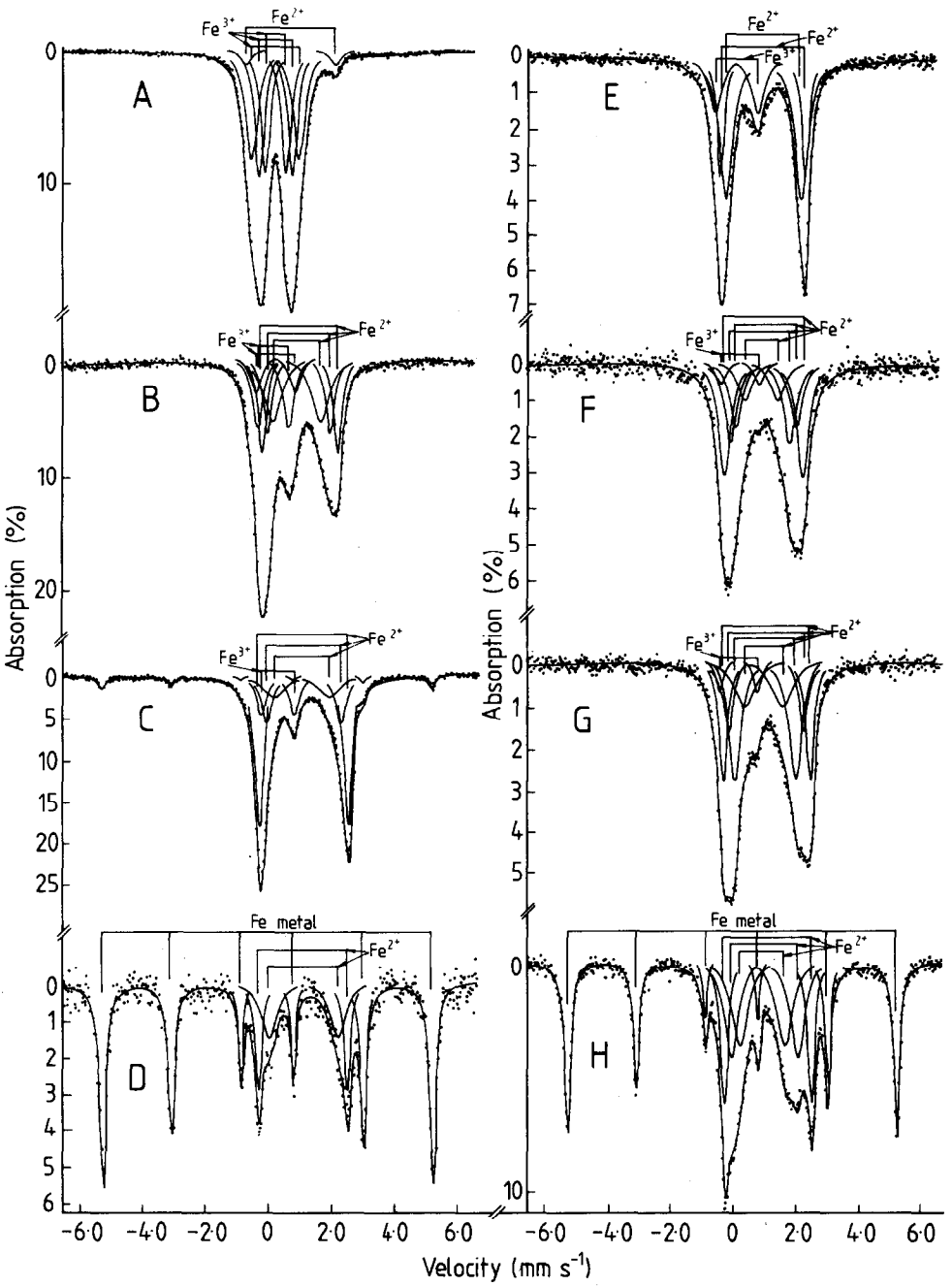

Fig. 8. Typical room-temperature Mössbauer spectra of berthierines heated in H_2/N_2. A–D, Sample B1 (Norway); E–H, sample B2 (Japan). A, 200–300°C; B, 400–500°C; C, 700°C; D, 1000–1200°C; E, 200–450°C; F, 600°C; G, 800°C; H, 1000–1200°C.

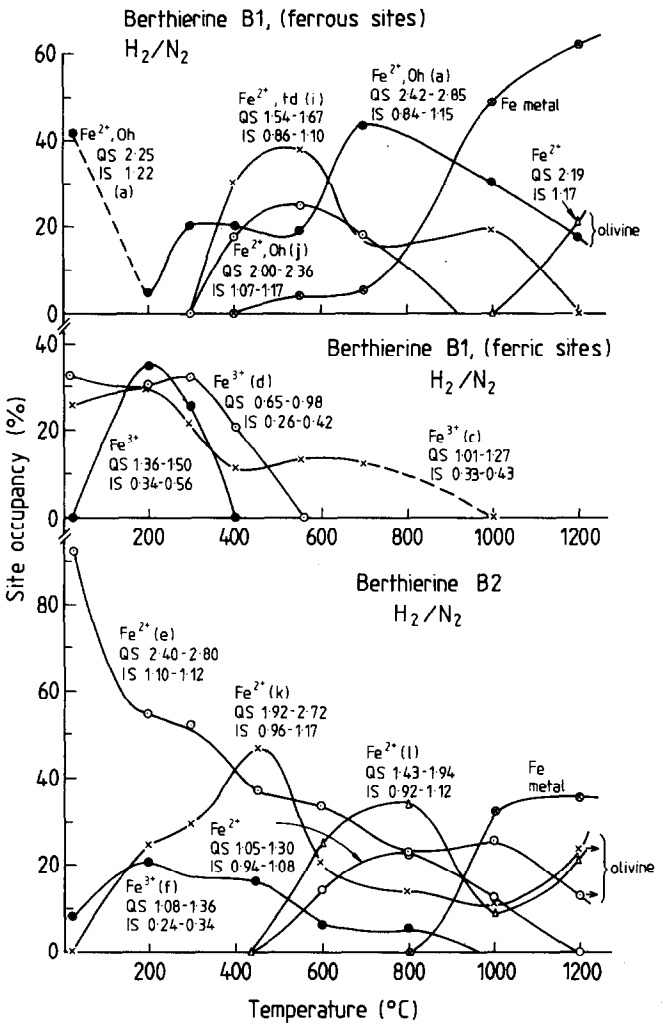

Fig. 9. Iron site occupancy changes in berthierines heated in H_2/N_2, deduced from Mössbauer peak areas. Isomer shifts quoted with respect to iron metal.

distorted octahedral site appears, and is re-reduced at 300–400°C, simultaneously with the reduction of the original Fe^{3+} sites c and d to new Fe^{2+} doublets i and j (Fig. 9). The parameters of i and j are characteristic of tetrahedral and octahedral Fe^{2+}, respectively. At higher temperatures, iron metal forms at the expense of all the Fe^{2+} doublets which become progressively less intense, but even at 1200°C, two Fe^{2+} sites persist (Fig. 9). The site with the larger QS is related to the original ferrous a site, but the other is a new resonance, replacing the tetrahedral Fe^{2+} site i. The parameters of these doublets are similar to those reported for the M1 and M2 sites of magnesium-substituted fayalite (IS = 1.03, QS = 2.41 and IS = 0.89, QS =

2.14 mm s^{-1}, respectively [26]), consistent with the X-ray results for reduced B1.

In B2, the Fe^{3+} doublet f behaves similarly to doublet c in B1, initially increasing in intensity, then gradually disappearing. As reduction proceeds, a new octahedral Fe^{2+} resonance k grows at the expense of the Fe^{2+} doublet e, eventually becoming the M2 olivine site (Fig. 9). On the completion of dehydroxylation, two additional Fe^{2+} doublets are resolved; one is transitory, but the other (l), with characteristically tetrahedral parameters, progressively intensifies up to 1200°C. This resonance could be due to iron in either of the high-temperature products ferroan cordierite or the cubic phase $(Mg,Fe)_2SiO_4$. The Fe^{2+} in cordierite is predominantly octahedral, with QS = ~ 2.3 mm s^{-1} [27]. Although the Mössbauer spectrum of cubic $(Mg,Fe)_2SiO_4$ is unknown, the Fe^{2+}-containing spinels $(Mg,Fe)Al_2O_4$ and $FeAl_2O_4$ both contain mainly tetrahedral Fe^{2+}, with parameters (IS = 0.89, QS = ~ 1.36 mm s^{-1} [28]) similar to those of doublet l. The identification of doublet l in B2 (and, by analogy, doublet i in B1) with Fe^{2+} in the spinel phase is consistent with the disappearance of doublet i from B1 at 1200°C, coincident with the disappearance of cubic $(Mg, Fe)_2SiO_4$ (Fig. 3).

(e) Mechanistic implications

Structurally, berthierine can be regarded as an amesite in which most of the octahedral Mg has been replaced by Fe^{2+}. Amesite decomposes in a similar manner to serpentines, which form crystalline products immediately on dehydroxylation. The primary recrystallization product of amesite is a spinel which subsequently transforms to related cubic phases [8]. Although the berthierine structure can tolerate significant amounts of octahedral Fe^{3+} so long as hydroxyl groups are also present, full dehydroxylation produces immediate structural breakdown, the products depending on the amount of octahedral Al present. In air, the more highly aluminous B2 forms an X-ray amorphous phase, stable over a range of ~ 200°C, in this respect behaving similarly to kaolinite, in which the octahedral sites are fully occupied by Al. By contrast, in air the less-highly aluminous B1 forms Fe_2O_3 and a non-crystalline siliceous component immediately on dehydroxylation. This reaction is similar to that of cronstedtite in air [13], although the transitory silicon-containing hematite precursor formed in cronstedtite was not found in berthierine, consistent with the relatively small degree of replacement of tetrahedral Al by Fe^{3+} in berthierine by comparison with cronstedtite. Under reducing conditions, the decomposition of berthierine is again sensitive to the octahedral Al content; B2 forms an amorphous phase which eventually recrystallizes to products which include a silicate spinel (as in kaolinite) whereas B1 behaves more like a serpentine, forming olivine immediately on dehydroxylation. These results are also consistent with the earlier findings of Brindley and Youell [3] who reported the formation in air

or vacuum of an X-ray amorphous intermediate in a British berthierine with an Al_2O_3 content of 21.82%, similar to the present B2.

CONCLUSIONS

When heated under oxidising or reducing conditions, the present berthierines undergo the following changes.

Below ~ 250°C. Internal oxidation of the octahedral ferrous iron leads to the formation of ferric berthierine, with a decreased cell volume reflecting decreases in the cell parameters. The IR spectra of samples heated in air indicate progressive ferric-for-ferrous substitution; a similar IR result is found for B1 in H_2/N_2, but not for the more aluminous B2, in which the cell volume changes are also less pronounced. The Fe^{3+} resulting from internal oxidation is in distorted octahedral sites which in B1 are distinct from the Fe^{3+} sites present in the unheated material. In B2, the population of Fe^{3+} sites in the unheated material progressively increases with oxidation, suggesting that the unheated sample has already undergone a small degree of internal oxidation.

200–400°C. In H_2/N_2, re-reduction occurs, with an increase in cell parameters, and, in B1, the re-population of the original Fe^{2+} sites and a return to the typical ferrous berthierine IR spectrum. By comparison, the original Fe^{2+} sites in B2 are not re-populated, but a new Fe^{2+} resonance develops which eventually becomes one of the olivine resonances.

~ 400–700°C. Dehydroxylation occurs, with the immediate formation of crystalline phases in B1. In B2, an X-ray-amorphous state occurs, which persists to 800–900°C before transforming to crystalline products. In this respect, B1 behaves more like a serpentine and the more aluminous B2 is like a kaolinite. The IR and Mössbauer spectra undergo no dramatic changes during dehydroxylation.

800–1200°C. The products become more crystalline, with characteristic IR and Mössbauer spectra. In air, the products are predominantly hematite (Fe_2O_3), cristobalite (SiO_2) and an iron-containing spinel phase, the more aluminous B2 also containing $FeAlO_3$ and mullite ($Al_6Si_2O_{13}$). In H_2/N_2, the major phases are iron metal and olivine, $(Fe, Mg)_2SiO_4$, which also occurs in a cubic form. A small amount of iron-substituted cordierite also forms latterly. No evidence was found for the transitory formation of magnetite, as previously postulated [4].

ACKNOWLEDGEMENTS

We are indebted to Dr. P.G. Embrey (British Museum) and Prof. A. Iijima (Geological Institute, University of Tokyo) for the berthierine sam-

ples, Dr. J.H. Johnston for the use of the Mössbauer spectrometer, Dr. L.M. Parker for the evolved gas analyses, Mr. M.W. Dwyer for the chemical analysis of B1, and Mr. M.E. Bowden for technical assistance.

REFERENCES

1 G.W. Brindley, Mineral. Mag., 29 (1951) 502.
2 B.W. Nelson and R. Roy, Am. Mineral., 43 (1958) 707.
3 G.W. Brindley and R.F. Youell, Mineral. Mag., 30 (1953) 57.
4 M. Escoubes and M.M. Karchoud, Bull. Soc. Fr. Ceram., 114 (1977) 43.
5 C.E. Weaver, J.M. Wampler and T.E. Pecuil, Science, 156 (1961) 504.
6 J.M.D. Coey, O. Ballet, A. Moukarika and J.L. Soubeyroux, Phys. Chem. Miner., 7 (1981) 141.
7 Z.P. Yershova, A.P. Nikitina, Yu. D. Perfil'ev and A.M. Babeshkin, Proc. Int. Clay Conf., Mexico City, 1975, p. 211.
8 K.J.D. MacKenzie and M.E. Bowden, Thermochim. Acta, 64 (1983) 83.
9 A. Iijima and R. Matsumoto, Clays. Clay. Miner., 30 (1982) 264.
10 R.C. MacKenzie (Ed.), The Differential Thermal Investigation of Clays, Min. Soc. Monograph, London, 1957, p. 222.
11 H.T. Evans, D.E. Appleman and D.S. Handwerker, Ann. Meeting Am. Cryst. Assoc., 1963, p. 42.
12 H. Kodama and A.E. Foscolos, Can. Mineral., 19 (1981) 279.
13 K.J.D. MacKenzie and R.M. Berezowski, Thermochim. Acta, 44 (1981) 171.
14 B.W. Nelson and R. Roy, Clays Clay Miner., Nat. Acad. Sci. Nat. Res. Council Pub., 327 (1954) 335.
15 J.A. Gadsen, Infrared Spectra of Minerals and Related Inorganic Compounds, Butterworth, London, 1975, p. 211.
16 C.J. Serna, B.D. Velde and J.L. White, Am. Mineral., 62 (1977) 296.
17 V. Stubican and R. Roy, J. Am. Ceram. Soc., 44 (1961) 625.
18 V.C. Farmer (Ed.), The Infrared Spectra of Minerals, Mineral Soc. Monograph No. 4, London, 1974.
19 H. Shirozu and K. Ishida, Mineral. J., 11 (1982) 161.
20 R. Jeanloz, Phys. Chem. Mineral., 5 (1980) 327.
21 O.K. Borggard, H.B. Lindgreen and S. Mørup, Clays. Clay Mineral., 30 (1982) 353.
22 T. Ericsson, R. Wappling and K. Punakivi, Geol. Foeren. Stockholm Foerh., 99 (1977) 229.
23 B.A. Goodman and D.C. Bain, in M.M. Mortland and V.C. Farmer (Eds.), Proc. Int. Clay Conf., Oxford, 1978, Elsevier, Amsterdam, 1979, p. 65.
24 T.V. Malysheva, L.M. Satarova and N.P. Palyakova, Geochem. Int., 14 (1977) 117.
25 K.J.D. MacKenzie and I.W.M. Brown, J. Mater. Sci. Lett., in press.
26 W.R. Bush, S.S. Hafner and D. Virgo, Nature (London), 227 (1970) 1339.
27 J.F. Duncan and J.H. Johnston, Aust. J. Chem., 27 (1974) 249.
28 B.L. Dickson and G. Smith, Can. Mineral., 14 (1976) 206.